Analysis of the tilted flat punch in couple-stress elasticity

P.A. Gourgiotis[1], Th. Zisis[2] and K.P Baxevanakis[3]

[1] *Department of Civil, Environmental and Mechanical Engineering, University of Trento, Trento, I-3812, Italy*

[2] *Mechanics Division, National Technical University of Athens, Zographou, GR-15773, Greece*

[3] *Mechanical Engineering & Mechanics Department, Drexel University, Philadelphia, PA 19104, USA*

Abstract. In the present paper we explore the response of a half-plane indented by a tilted flat punch with sharp corners in the context of couple-stress elasticity theory. Contact conditions arise in a number of modern engineering applications ranging from structural and geotechnical engineering to micro and nanotechnology. As the contact scales reduce progressively the effects of the microstructure upon the macroscopic material response cannot be ignored. The generalized continuum theory of couple-stress elasticity introduces characteristic material lengths in order to describe the pertinent scale effects that emerge from the underlying material microstructure. The problem under investigation is interesting for three reasons: Firstly, the indentor's geometry is simple so that benchmark results may be extracted. Secondly, important deterioration of the macroscopic results may emerge in the case that a tilting moment is applied on the indentor inadvertently or in the case that the flat punch itself is not self-aligning so that asymmetrical contact pressure distributions arise on the contact faces. Thirdly, the voluntary application of a tilting moment on the flat punch during an experiment gives rise to potential capabilities of the flat punch for the determination of the material microstructural characteristic lengths. The solution methodology is based on singular integral equations which have resulted from a treatment of the mixed boundary value problems via integral transforms and generalized functions. The results show significant departure from the predictions of classical elasticity revealing that valuable information may be deducted from the indentation of a tilted punch of a microstructured solid.

Keywords: micromechanics, complete contact, receding contact, indentation, tilt angle, singular integral equations

* Corresponding author: Tel.: +39 0461 282594; Fax: +39 0461 282599.

E-mail address: p.gourgiotis@unitn.it (Panos A. Gourgiotis)

1. Introduction

Contact situations occur in a multitude of engineering applications ranging from mechanical and civil engineering to materials science. Many structures are founded in reinforced concrete footings or pads buried at relatively shallow depths beneath the ground surface and large scale contacts take place between the footings and the deformable ground. On the other hand, small scale contacts appear in nano-indentation tests in the area of mechanical engineering and/or material science.

In an ideal contact situation between two bodies, either within the context of civil engineering where the footing essentially acts as an indentor that lies upon a deformable body (i.e. the ground) or within the spirit of an indentation experiment where the flat surface of the underlying material is mounted perpendicular to the tip of the indentor, the indentor touches the surface of the material and penetration is performed. The details of such penetration may be interpreted in terms of the stress distribution below the indentor and subsequently the stress distribution within the bodies in contact, the surface displacements, the contact site, etc. Such analysis is crucial for design purposes in geotechnical and footing engineering, or in the case of material characterization through indentation tests.

During contact conditions, size effects can be dominant especially when the contact size (that is the contact area) is comparable to the material microstructure. However, it is well known that the classical continuum theory possesses no intrinsic length scale and thus fail to predict the scale effects observed experimentally in indentation problems with geometric lengths comparable to the lengths of the material microstructure (e.g. Fleck and Hutchinson, 2001). This discrepancy between the classical theoretical predictions and experimental results is found more pronounced for materials with a coarse-grain structure. In fact, the macroscopical behavior of most microstructured materials with non-homogeneous microstructure, like ceramics, composites, cellular materials, foams, masonry, bone tissues, glassy and semi-crystalline polymers, is strongly influenced by the microstructural characteristic lengths, especially in the presence of large stress (or strain) gradients (Maranganti and Sharma 2007).

In order to study the size effects observed during indentation of microstructured materials two different approaches may be followed. The first one consists of taking into account the distinct morphology of the material through discrete modelling and incorporating directly the details of the material microstructure. This approach, although very detailed and accurate, suffers since the computational cost becomes increasingly high with increasing material complexity. The alternative is the use of a generalized continuum theory that smears out the material microstructure by enriching

the classical continuum with additional material characteristic length scales extending, thus, the range of applicability of the 'continuum' concept in an effort to bridge the gap between classical continuum theories and atomic-lattice theories. This approach is very effective since it can be incorporated efficiently into large computations but of course lacks the detailed description of a discrete representation and treats the microstructural length in an average sense. Discrete modelling of the material microstructure during indentation has been carried in the context of classical continuum theories (see e.g. Chen et al., 2004; Stupkiewicz, 2007; Fleck and Zisis, 2010; Zisis and Fleck, 2010), whereas phenomenological approaches based on generalized continua have also been extensively followed (Muki and Sternberg, 1965; Poole et al., 1996; Begley and Hutchinson, 1998; Nix and Gao, 1998; Shu and Fleck, 1998; Wei and Hutchinson, 2003; Zisis et al., 2014).

The physical relevance of the material length scales as introduced through generalized continuum theories has been the subject of numerous theoretical and experimental studies. Chen et al. (1998) developed a continuum model for cellular materials and concluded that the continuum description of these materials obeys a gradient elasticity theory of the couple-stress type. In the latter study, the intrinsic material length was naturally identified with the cell size. Furthermore, regarding cellular solids, Tekoglu and Onck (2008) compared the analytical results of various gradient type generalized continuum theories with the computational results of discrete models through a range of basic boundary value problems based on Voronoi representations of cellular microstructures. The analysis that was performed, strictly within the elastic regime, assessed the capabilities of generalized continuum theories in capturing size effects in cellular solids and connected the cell size with the microstructural length-scale. Additionally, recent studies by Bigoni and Drugan (2007), and Bacca et al. (2013) provided an account of the determination of the couple-stress moduli via homogenization of heterogeneous materials. Moreover, Shodja et al. (2013) utilizing ab initio DFT calculations evaluated the characteristic material lengths of the gradient elasticity theory for several fcc and bcc metal crystals.

One of the most effective generalized continuum theories has proved to be that of couple-stress elasticity, also known as Cosserat theory with constrained rotations (Mindlin and Tiersten, 1962; Toupin, 1964). In the context of couple-stress elasticity, the strain-energy density and the resulting constitutive relations involve, besides the usual infinitesimal strains, certain strain gradients known as the rotation gradients. The generalized stress-strain relations for the isotropic case include, in addition to the conventional pair of elastic constants, two new elastic constants, one of which is expressible in terms of a material parameter ℓ that has dimension of [length]. The presence of this

length parameter, in turn, implies that the modified theory encompasses the analytical possibility of size effects, which are absent in the classical theory.

Even though, purely elastic indentation of materials is hard to achieve in practice (Larsson et al., 1996), elasticity can be of interest in particular cases of indentation. In fact, as it was shown by Han and Nikolov (2007), there are polymers that exhibit significant size effects during indentation also in the elastic regime. More specifically, indentation experiments with a Berkovich indentor carried out on heterochain polymers such as polycarbonate (PC), epoxy, polyethylene terephthalate (PET) and polyamide 66 or nylon66 (PP66), showed an increased hardness with decreasing indentation depths. Furthermore, Han and Nikolov (2007) reported that the depth at which the hardness starts to increase depends strongly, in the elastic deformation regime, upon the type of the polymer under consideration. In particular, they reported that the hardness at small indentation depths (or small contact areas) can increase from 0% to as much as 300%.

In the present paper, we explore the response of a half-plane indented by a tilted flat punch with sharp corners in the context of couple-stress elasticity theory. The same problem was initially studied by Sackfield et al. (2001) in the context of classical elasticity. Here, we extend their work and generalize their results for the case of a microstructured elastic material. The problem under investigation is of both theoretical and practical importance. From the theoretical point of view the indentor's geometry is very simple so that benchmark results may be extracted. From the practical point of view even with nominally symmetrical contacts there is a possible effect of a relative indentor's rotation as a result of an applied moment or an undesirable geometrical asymmetry. Non-symmetrical contact conditions may occur in materials science applications (i.e. indentation tests) when for example the properties of a material are extracted through the indentation technique. Similar asymmetries can also be found in large scale contact situations in civil engineering and in geotechnical applications where the footings essentially act as rigid indentors of the ground. If the tilting moment appears on the indentor inadvertently (possibly through the application of an offset force), then important deterioration of the contact results may emerge and significant macroscopic errors may occur. On the other hand, when a tilting moment on a flat punch is voluntarily applied, during for example an indentation experiment for material properties extraction, it gives rise to potential advantages regarding the capabilities of the flat punch, for the identification of the influence of the length scale effect through simple procedures (Lakes et al., 1985).

2. Basic equations of couple-stress elasticity in plane-strain

In this section, we recall briefly the main features of the equilibrium theory of plane strain within the linearized couple-stress theory of homogeneous and isotropic elastic solids. Detailed presentations of the couple-stress theory can be found in the fundamental papers of Mindlin and Tiersten (1962), and Koiter (1964). An exposition of the theory under plane-strain conditions was given in the work by Muki and Sternberg (1965), and more recently by Gourgiotis and Piccolroaz (2014) in the elastodynamic case including micro-inertial effects.

For a body that occupies a domain in the (x,y)-plane under conditions of plane-strain, the equations of equilibrium in the absence of body forces and body moments reduce to

$$\frac{\partial \sigma_{xx}}{\partial x}+\frac{\partial \sigma_{yx}}{\partial y}=0\,,\qquad \frac{\partial \sigma_{xy}}{\partial x}+\frac{\partial \sigma_{yy}}{\partial y}=0\,,\qquad \sigma_{xy}-\sigma_{yx}+\frac{\partial m_{xz}}{\partial x}+\frac{\partial m_{yz}}{\partial y}=0\,, \tag{1}$$

where ($\sigma_{xx},\sigma_{xy},\sigma_{yx},\sigma_{yy}$) and ($m_{xz},m_{yz}$) are the non-vanishing components of the (asymmetric) stress and couple-stress tensors, respectively. The complete solution of Eqs. (1) admits the following representation in terms of two sufficiently smooth stress functions $\Phi\equiv\Phi(x,y)$ and $\Psi\equiv\Psi(x,y)$ (Mindlin, 1963)

$$\begin{aligned}
&\sigma_{xx}=\frac{\partial^2\Phi}{\partial y^2}-\frac{\partial^2\Psi}{\partial x\partial y}\,,\quad \sigma_{yy}=\frac{\partial^2\Phi}{\partial x^2}+\frac{\partial^2\Psi}{\partial x\partial y}\,,\\
&\sigma_{xy}=-\frac{\partial^2\Phi}{\partial x\partial y}-\frac{\partial^2\Psi}{\partial y^2}\,,\quad \sigma_{yx}=-\frac{\partial^2\Phi}{\partial x\partial y}+\frac{\partial^2\Psi}{\partial x^2}\,,
\end{aligned} \tag{2}$$

and

$$m_{xz}=\frac{\partial\Psi}{\partial x}\,,\quad m_{yz}=\frac{\partial\Psi}{\partial y}\,. \tag{3}$$

Accordingly, the displacement field assumes the general form

$$u_x\equiv u_x(x,y)\,,\quad u_y\equiv u_y(x,y)\,,\quad u_z\equiv 0\,. \tag{4}$$

The governing kinematic relations in the framework of the geometrically linear theory then become

$$\varepsilon_{xx}=\frac{\partial u_x}{\partial x},\quad \varepsilon_{yy}=\frac{\partial u_y}{\partial y},\quad \varepsilon_{xy}=\varepsilon_{yx}=\frac{1}{2}\left(\frac{\partial u_y}{\partial x}+\frac{\partial u_x}{\partial y}\right), \tag{5}$$

$$\omega=\frac{1}{2}\left(\frac{\partial u_y}{\partial x}-\frac{\partial u_x}{\partial y}\right),\quad \kappa_{xz}=\frac{\partial \omega}{\partial x},\quad \kappa_{yz}=\frac{\partial \omega}{\partial y}, \tag{6}$$

where $\boldsymbol{\varepsilon}$ is the usual strain tensor, ω is the rotation, and $\left(\kappa_{xz},\kappa_{yz}\right)$ are the non-vanishing components of the curvature tensor (i.e. the gradient of rotation) expressed in dimensions of [length]$^{-1}$.

For a homogeneous and isotropic couple-stress material the constitutive equations furnish

$$\varepsilon_{xx}=\left(2\mu\right)^{-1}\left[\,\sigma_{xx}-\nu\left(\sigma_{xx}+\sigma_{yy}\right)\right],\ \varepsilon_{yy}=\left(2\mu\right)^{-1}\left[\,\sigma_{yy}-\nu\left(\sigma_{xx}+\sigma_{yy}\right)\right],$$
$$\varepsilon_{xy}=\left(4\mu\right)^{-1}\left(\sigma_{xy}+\sigma_{yx}\right), \tag{7}$$

and

$$\kappa_{xz}=\left(4\mu\ell^2\right)^{-1}m_{xz},\quad \kappa_{yz}=\left(4\mu\ell^2\right)^{-1}m_{yz}, \tag{8}$$

where μ, ν, and ℓ, stand for the shear modulus, Poisson's ratio, and the characteristic material length of couple-stress theory, respectively (Mindlin and Tiersten, 1962).

Further, substitution of Eqs. (2) and (3) into (7) and (8) results in the compatibility equations for the Mindlin's stress functions

$$\frac{\partial}{\partial x}\left(\Psi-\ell^2\nabla^2\Psi\right)=-2\left(1-\nu\right)\ell^2\nabla^2\left(\frac{\partial\Phi}{\partial y}\right), \tag{9}$$

$$\frac{\partial}{\partial y}\left(\Psi-\ell^2\nabla^2\Psi\right)=2\left(1-\nu\right)\ell^2\nabla^2\left(\frac{\partial\Phi}{\partial x}\right), \tag{10}$$

from which, in turn, we obtain the following uncoupled partial differential equations

$$\nabla^4 \Phi = 0\,, \tag{11}$$

$$\nabla^2 \Psi - \ell^2 \nabla^4 \Psi = 0\,. \tag{12}$$

Note that as the quantities ℓ, $\partial\Psi/\partial x$, and $\partial\Psi/\partial y$ tend to zero, the above representation passes over into the classical Airy's representation.

Finally, combining Eqs. (2)-(7), one can obtain the following relations expressing the displacement gradients in terms of the Mindlin's stress functions

$$\frac{\partial u_x}{\partial x} = \frac{1}{2\mu}\left(\frac{\partial^2 \Phi}{\partial y^2} - \frac{\partial^2 \Psi}{\partial x \partial y} - \nu \nabla^2 \Phi \right), \tag{13}$$

$$\frac{\partial u_y}{\partial y} = \frac{1}{2\mu}\left(\frac{\partial^2 \Phi}{\partial x^2} + \frac{\partial^2 \Psi}{\partial x \partial y} - \nu \nabla^2 \Phi \right), \tag{14}$$

$$\frac{\partial u_x}{\partial y} + \frac{\partial u_y}{\partial x} = -\frac{1}{2\mu}\left(2\frac{\partial^2 \Phi}{\partial x \partial y} - \frac{\partial^2 \Psi}{\partial x^2} + \frac{\partial^2 \Psi}{\partial y^2} \right). \tag{15}$$

3. Formulation of the contact problem and boundary conditions

The contact problem of a rigid indentor pressed into the surface of an elastic half-plane is now investigated. The body is governed by the equations of couple-stress elasticity and a Cartesian coordinate system $Oxyz$ is attached at the center line of the geometry, as shown in Figure 1. A load P is applied to the indentor which, in the plane strain case, has dimensions of [force][length]$^{-1}$.

It is assumed that the punch has a flat base of width $2b$ and sharp square corners; it is sufficiently long in the z-direction so that plane strain conditions prevail. Since the punch is rigid, the surface of the elastic solid must remain flat where it is in contact with the punch. The punch is tilted *counterclockwise* under the application of a load P which is shifted from the center line by a positive distance e (eccentricity). The problem may then be accordingly considered as the equivalent of a punch subjected to a normal load P and a moment $M = -Pe$. Depending on the magnitude of the applied moment, complete or receding type of contact may occur (Figure 1). In the case of complete contact, the contact region consists of the points: $D \equiv \{(x,y): -b \le x \le b,\ y = 0\}$ and the contact width is $c = 2b$. In the case receding contact, the contact region consists of the points:

$D \equiv \{(x,y): -b \le x \le a,\ y = 0\}$ and the contact width is $c = a + b$, with $|a| < b$. Note that in all cases,

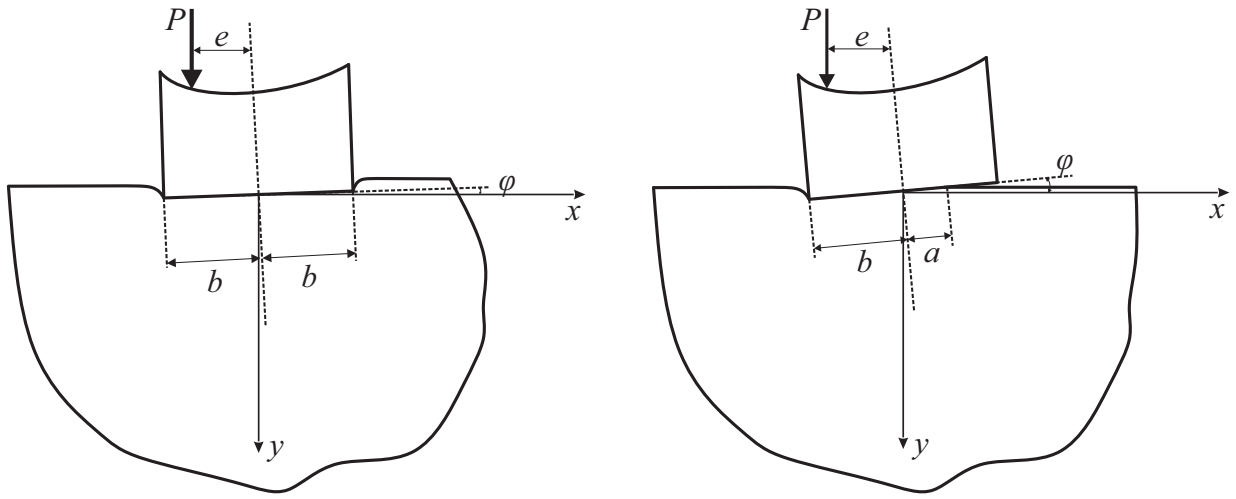

(a) **(b)**

Figure 1: The tilted punch under **(a)** complete contact; the contact width is $c = 2b$ (b is the half width of the flat punch), and **(b)** receding contact; the contact width is $c = a + b$.

For the points lying within the contact region $x \in D$ after loading, we have the following general geometrical boundary condition

$$u_y = \delta - \varphi x, \tag{16}$$

where, φ is the angle of inclination of the tilted punch which is sufficiently small for the linear small strain elasticity to applicable, and δ is a positive constant acting as a measure of the absolute approach of the contacting bodies. Furthermore, the following traction boundary conditions hold for a frictionless and smooth type of contact (Shu and Fleck, 1998; Zisis et al. 2014)

$$\sigma_{yy}(x,0) = 0 \quad \text{for} \quad x \notin D\ , \tag{17}$$

$$\sigma_{yx}(x,0) = 0 \quad \text{for} \quad -\infty < x < \infty\ , \tag{18}$$

$$m_{yz}(x,0) = 0 \quad \text{for} \quad -\infty < x < \infty\ , \tag{19}$$

which are accompanied by the *auxiliary* conditions

$$\int_D \sigma_{yy}(x,0)\,dx = -\int_D p(x)\,dx = -P, \tag{20}$$

and

$$\int_D \sigma_{yy}(x,0)\,x\,dx = -\int_D p(x)\,x\,dx = -M, \tag{21}$$

where $p(x) \geq 0$ is the pressure below the indentor, P is the applied load, and M is the applied moment. Moreover, since the indented surface is an unbounded region, the above boundary conditions must be supplemented by the regularity conditions at infinity

$$\sigma_{ij} \to 0, \;\; m_{ij} \to 0 \quad \text{as} \quad R = \left(x^2 + y^2\right)^{1/2} \to \infty. \tag{22}$$

4. Singular integral equation approach

The plane-strain contact problem is attacked with the aid of the Fourier transform on the basis of the stress function formulation summarized earlier. The direct Fourier transform and its inverse are defined as follows

$$\hat{f}(\xi) = \int_{-\infty}^{\infty} f(x) e^{i\xi x} dx \quad , \quad f(x) = \frac{1}{2\pi}\int_{-\infty}^{\infty} \hat{f}(\xi) e^{-i\xi x} d\xi \;, \tag{23}$$

where $i \equiv (-1)^{1/2}$.

Transforming the governing equations (11) and (12) with $(23)_1$ provides a pair of fourth order ODEs with constant coefficients whose solution is immediate. The constants that emerge may be subsequently be evaluated from the transform of Eqs (9) and (10) in conjunction with the transformed boundary conditions (17)-(19). Since the procedure just outlined is strictly analogous to that employed in Zisis et al. (2014), we may omit the details of the analysis and cite directly the results obtained. In particular, the transformed stress functions assume now the following form

$$\hat{\Phi}(\xi,y)=\left[1+\frac{|\xi|\gamma y}{\gamma-4(1-\nu)\ell^2\xi^2\left(|\xi|-\gamma\right)}\right]\frac{e^{-|\xi|y}}{\xi^2}\hat{p}(\xi), \tag{24}$$

$$\hat{\Psi}(\xi,y)=-\frac{4i\ell^2(1-\nu)\left[|\xi|\gamma e^{-|\xi|y}-\xi^2e^{-\gamma y}\right]}{\left[\gamma-4(1-\nu)\ell^2\xi^2\left(|\xi|-\gamma\right)\right]\xi}\hat{p}(\xi), \tag{25}$$

where $\gamma\equiv\gamma(\xi)=\left(\ell^{-2}+\xi^2\right)^{1/2}$ and $\hat{p}(\xi)$ is the transformed pressure distribution below the indentor which, taking also into account Eq. (17), can be written as

$$\hat{p}(\xi)=\int_D p(x)e^{i\xi x}dx. \tag{26}$$

Finally, in view of (13)-(15), the displacements in the transformed domain become

$$\hat{u}_x=\frac{1}{2\mu\xi}\left(i(1-\nu)\frac{d^2\hat{\Phi}}{dy^2}-\xi\frac{d\hat{\Psi}}{dy}+i\nu\xi^2\hat{\Phi}\right),$$

$$\hat{u}_y=\frac{1}{2\mu\xi^2}\left((1-\nu)\frac{d^3\hat{\Phi}}{dy^3}-(2-\nu)\xi^2\frac{d\hat{\Phi}}{dy}-i\xi^3\hat{\Psi}\right). \tag{27}$$

Our objective now is the determination of the contact-stress distribution $p(x)$ under the indentor and the determination of the pertinent contact width when appropriate. For the solution of the mixed boundary value problem, we employ the method of singular integral equations. In classical elasticity, the general procedure of reducing mixed boundary value problems to singular integral equations is given, e.g., by Erdogan (1978), Hills and Nowell (1994). An application of the technique within the context of couple-stress elasticity for plane-strain contact problems can be found in Zisis et al. (2014).

The definition of the inverse Fourier transform in (23) together with the second of (27) lead to following equation

$$\frac{du_y}{dx}=\frac{1}{2\pi}\int_{-\infty}^{\infty}\left[\frac{-i}{2\mu\xi}\left((1-\nu)\frac{d^3\hat{\Phi}}{dy^3}-(2-\nu)\xi^2\frac{d\hat{\Phi}}{dy}-i\xi^3\hat{\Psi}\right)\right]e^{-ix\xi}d\xi, \tag{28}$$

which, by using the expressions for the stress functions (24) and (25) at $y=0$ and bearing in mind Eq. (26), yields

$$\frac{du_y}{dx}=\frac{1}{2\pi}\int_{-\infty}^{\infty}\frac{i(1-\nu)|\xi|\gamma}{\mu\xi\left[4(1-\nu)\ell^2\xi^2\left(|\xi|-\gamma\right)-\gamma\right]}\cdot\left[\int_D p(t)e^{i\xi t}dt\right]e^{-ix\xi}d\xi\,. \tag{29}$$

Further, employing the displacement boundary condition in (16) and reversing the order of integration in (29), the problem is reduced to the following integral equation

$$\int_D p(t)K(x-t)dt=-\mu\pi\varphi,\quad x\in D \tag{30}$$

where the kernel $K(x-t)$ is defined as

$$K(x-t)=\int_0^{\infty}g(\xi)\sin\left(\xi(x-t)\right)d\xi\,, \tag{31}$$

with

$$g(\xi)=\frac{(1-\nu)\gamma}{4(1-\nu)\ell^2\xi^2(\xi-\gamma)-\gamma}\,. \tag{32}$$

It is worth noting that passing to the limit as $\ell\to 0$ in Eq. (30), one recovers the integral equation that governs the respective contact problem in classical elasticity.

For the solution of the integral equation (30), it is expedient to separate the kernel to its singular and regular parts. To this purpose, we examine the asymptotic behavior of the function $g(\xi)$ as $\xi\to\infty$ by using the Abel–Tauber theorem. In particular, noting that $\lim\limits_{\xi\to\infty}g(\xi)=g_\infty(\xi)=-\dfrac{1-\nu}{3-2\nu}$, the function $g(\xi)$ is decomposed as

$$g(\xi)=g_\infty(\xi)+\left[g(\xi)-g_\infty(\xi)\right], \tag{33}$$

and, accordingly, the kernel $K(x-t)$ becomes

$$K(x-t)=\underbrace{\int_0^\infty g_\infty(\xi)\sin\big(\xi(x-t)\big)d\xi}_{\text{singular part}}+\underbrace{\int_0^\infty\big[g(\xi)-g_\infty(\xi)\big]\sin\big(\xi(x-t)\big)d\xi}_{\text{regular part}}$$

$$=-\frac{(1-\nu)}{(3-2\nu)}\frac{1}{x-t}+N(x-t), \tag{34}$$

where

$$N(x-t)=\frac{2(1-\nu)^2}{(3-2\nu)}\int_0^\infty\left[\frac{\big(2\ell^2\xi^2(\gamma-\xi)-\gamma\big)}{\big(\gamma+4(1-\nu)\ell^2\xi^2(\gamma-\xi)\big)}\right]\sin\big(\xi(x-t)\big)d\xi, \tag{35}$$

is a regular square-integrable kernel.

To this end, the following normalizations are adopted

$$x=\frac{a+b}{2}(r+d),\quad t=\frac{a+b}{2}(s+d),\quad \xi=\frac{2}{a+b}\zeta,\quad \ell=\frac{a+b}{2}q. \tag{36}$$

with $d=(a-b)/(a+b)$. Accordingly, the governing singular integral equation for the pressure under the indentor assumes the following form

$$-\frac{(1-\nu)}{(3-2\nu)}\int_{-1}^{1}\frac{p(s)}{r-s}ds+\int_{-1}^{1}\tilde{N}(r-s)\,p(s)\,ds=-\mu\pi\varphi\ ,\quad |r|\le 1, \tag{37}$$

where the normalized regular kernel is defined now as

$$\tilde{N}(r-s)=\frac{2(1-\nu)^2}{(3-2\nu)}\int_0^\infty\left[\frac{\big(2q^2\zeta^2(\tilde{\gamma}-\zeta)-\tilde{\gamma}\big)}{\big(\tilde{\gamma}+4(1-\nu)q^2\zeta^2(\tilde{\gamma}-\zeta)\big)}\right]\sin\big(\zeta(r-s)\big)d\zeta, \tag{38}$$

with $\tilde{\gamma}=\left(\zeta^2+q^{-2}\right)^{1/2}$. Note that the first integral in the integral equation (37) is interpreted in the Cauchy principal value (CPV) sense. In fact, the CPV integral in Eq. (37) dominates the regular kernel and therefore determines the nature of the singularity of the pressure $p(s)$ at the endpoints of the contact region $r=\pm 1$. Therefore, guided also by the results concerning the modification of stress singularities in the presence of couple stresses (Muki and Sternberg, 1965; Zisis et al. 2014), a general solution for the pressure distribution admits the representation

$$p(s)=w(s)\cdot\sum_{j=0}^{\infty}B_j P_j^{(\alpha,\beta)}(s)\ ,\quad |s|\le 1\ , \tag{39}$$

where $P_j^{(\alpha,\beta)}(s)$ are the Jacobi polynomials orthogonal to the weight function

$$w(s)=(1-s)^{\alpha}(1+s)^{\beta}\ ,\quad (-1<(\alpha,\beta)<1\ ,\ |s|\le 1)\ . \tag{40}$$

with $\alpha=1/2+\mathrm{N}$, $\beta=-1/2+\mathrm{M}$, and (N,M) arbitrary integers. The parameters (α,β) depend upon the type of contact (complete or receding).

Employing now the well-known Gauss-Jacobi integration formulas for singular CPV integrals (Szegö, 1939; Erdogan et al., 1973; Hills et al., 1993), the integral equation (37) is reduced to a system of algebraic relations; viz.,

$$\sum_{j=0}^{\infty}B_j\left[-\frac{(1-\nu)}{(3-2\nu)}\frac{2^{-k}}{\sin\pi\alpha}P_{j-k}^{(-\alpha,-\beta)}(r)+Q_j(r)\right]=-\mu\varphi\ ,\quad |r|<1\ , \tag{41}$$

where $k=-\alpha-\beta$ is the index of the singular integral equation (37), and

$$Q_j(r)=\frac{1}{\pi}\int_{-1}^{1}w(s)P_j^{(\alpha,\beta)}(s)\tilde{N}(r-s)\,ds\ . \tag{42}$$

Furthermore, the auxiliary conditions (20) and (21) read

$$\int_{-1}^{1} p(s)\,ds = \frac{2P}{(a+b)}, \quad \int_{-1}^{1} p(s)\,s\,ds = \frac{4M + 2P(b-a)}{(a+b)^2}. \tag{43}$$

Two cases are now considered. In the first case, the applied moment is relatively small so that the contact is expected to be *complete* across the face of the punch ($c = 2b$, $a = b$). In the second case, the applied moment is sufficiently high, causing one corner of the punch to lift out of contact, and therefore for the contact extremity to be positioned at some point along the punch face ($c = a + b$, $|a| < b$) – see Figure 1b.

4.1 Complete contact

In this case, the pressure is singular at both ends of the contact width. Therefore, the weight function in Eq. (40) becomes: $w(s) = (1 - s^2)^{-1/2}$ (i.e. $\alpha = \beta = -1/2$). In addition, the auxiliary conditions (43) are simplified to the following form

$$\int_{-1}^{1} p(s)\,ds = \frac{P}{b}, \quad \int_{-1}^{1} p(s)\,s\,ds = \frac{M}{b^2}, \tag{44}$$

which, taking into account (39), imply that

$$B_0 = \frac{P}{\pi b}, \quad B_1 = \frac{4M}{\pi b^2}. \tag{45}$$

Note that in complete contact the regular integral in (42) is evaluated using the standard Gauss-Chebyshev quadrature method.

The system of equations (41) is solved by truncating the series at $j = n$ and using a collocation technique with collocation points chosen as the roots of the second kind Chebyshev polynomial $U_n(r)$, viz. $r_j = \cos\left(j\pi/(n+1)\right)$ with $j = 1, 2, ..., n$. In this way, a system of n linear algebraic equations is formed that enables us to evaluate the remaining n unknowns: the $n-1$ coefficients B_j ($j = 2, ..., n$) and the unknown tilt angle φ.

4.2 Transition from complete to receding contact

In order to define the critical moment M_{cr} at which the contact type changes from complete to receding, we use the same collocation scheme as in Section 4.1 combined with the additional condition that the pressure at the right end point of the indentor width ($r=1$) is equal to zero. In this way, a system of $n+1$ linear algebraic equations is formed that enables us to evaluate the remaining $n-1$ coefficients B_j ($j=2,...,n$), the tilt angle φ, and the critical moment M_{cr}.

4.3 Receding contact

In this case, the pressure is zero at the right end of the contact area, so that $\alpha=1/2$ and $\beta=-1/2$. Accordingly, the weight function becomes: $w(s)=(1-s)^{1/2}(1+s)^{-1/2}$ and the auxiliary conditions are given in Eqs. (43), which, in view of (39), imply that

$$B_0=\frac{2P}{\pi(a+b)}\ ,\quad B_1=\frac{4\big(4M+P(3b-a)\big)}{\pi(a+b)^2}. \tag{46}$$

The system of equations in (41) is now solved by using a collocation method with collocation points chosen as the roots of the Jacobi polynomial $P_{n+1}^{(-1/2,1/2)}(r)$, viz. $r_j=\cos\big((2j-1)\pi/(2n+3)\big)$ with $j=1,2,...,n+1$. Here, in order to derive results for *constant* ratio ℓ/b, we consider the contact length a as a prescribed quantity and let the eccentricity e to float. The resulting $n+1$ linear algebraic equations are then utilized in conjunction with Eqs. (46) to evaluate the coefficients B_j, the tilt angle φ, and the unknown eccentricity e.

5. Results and discussion

The discussion of the results obtained for the problem of the tilted flat punch under conditions of complete and receding contact is now in order. In what follows, special focus will be given to the effect of the ratio ℓ/b (normalized characteristic length) and the Poisson's ratio ν upon the contact pressure distribution $p(x)$, the contact width c, and the tilt angle φ. It is noted that although our results are presented in terms of the dimensionless ratio ℓ/b, the normalization $q=2\ell/c$ (Eq.(36)$_4$) could alternatively be adopted. In fact, the ratio q occurs naturally in the formulation of the integral equation (37), however, for practical applications the normalization ℓ/b is more suitable since it

involves the known geometrical characteristics of the indentor and the characteristic length of the couple-stress material.

5.1 Effect of the normalized characteristic length upon the contact pressure distribution

In Figure 2, we present selected characteristic pressure distributions below the indentor resulting from the application of the load P at various normalized eccentricities e/b from the center of the punch. Results are shown for the cases of classical elasticity $(\ell/b=0)$ and couple-stress elasticity for a material with $\ell/b=0.5$ and for two Poisson's ratios namely, $\nu=0$ and $\nu=0.5$. We begin by reporting some general results that correspond to the case of $e/b=0$ - the 'standard' flat punch indentation problem where no tilt is applied. As it has been shown by Muki and Sternberg (1967) and Zisis et al. (2014), when ℓ/b increases from zero the pressure distribution curves depart from and then again approach the classical elasticity result.

As the load is translated from the center line of the punch $(e/b>0)$ the pressure distribution curves change qualitatively. At $e/b=0.5$ and independently of the Poisson's ratio, the pressure distribution attained for the classical elasticity case (red line) suggests that the punch is at the limit between the complete and the receding contact regime. In this case, the classical pressure at the right corner of the punch reduces to zero while at the left corner it remains square-root singular. However, the pressure distribution that corresponds to the couple-stress elasticity case shows that the flat punch is still in complete contact for a material with $\ell/b=0.5$. Further increase of the load eccentricity implies that the contact characteristics change from complete to receding also in the couple-stress elasticity case. Note that, unlike the classical elasticity case, the limit eccentricity e^{lim} between complete to receding contact depends now, in addition to contact half-width b , upon the Poisson's ratio ν and the characteristic material length ℓ. Nonetheless, the limit eccentricity in couple-stress elasticity is *independent* of the magnitude of the load P, as in the classical theory (Sackfield et al. 2001). For example, when $\nu=0$ and $\ell/b=0.5$ the limit eccentricity is $e^{lim}=0.61b$. At this eccentricity, the contact region below the indentor for the classical elasticity case is equal to $c=1.59b$ (recall that $c=2b$ is the complete contact width). Larger values of eccentricity would produce receding contact conditions *both* in classical and in couple-stress theory and the contact widths would progressively reduce. This reduction is more pronounced for larger values of the Poisson's ratio. However, it should be mentioned that the difference in the extent of the receding contact region in couple-stress elasticity and in classical elasticity reduces as $e/b\to 1$. The response

is qualitatively similar to the case of an incompressible material $(\nu = 0.5)$ and for this reason no separate comment is required.

The above results imply that for the same eccentricity, greater resistance against the reduction of the contact width is observed when couple-stress effects are taken into account.

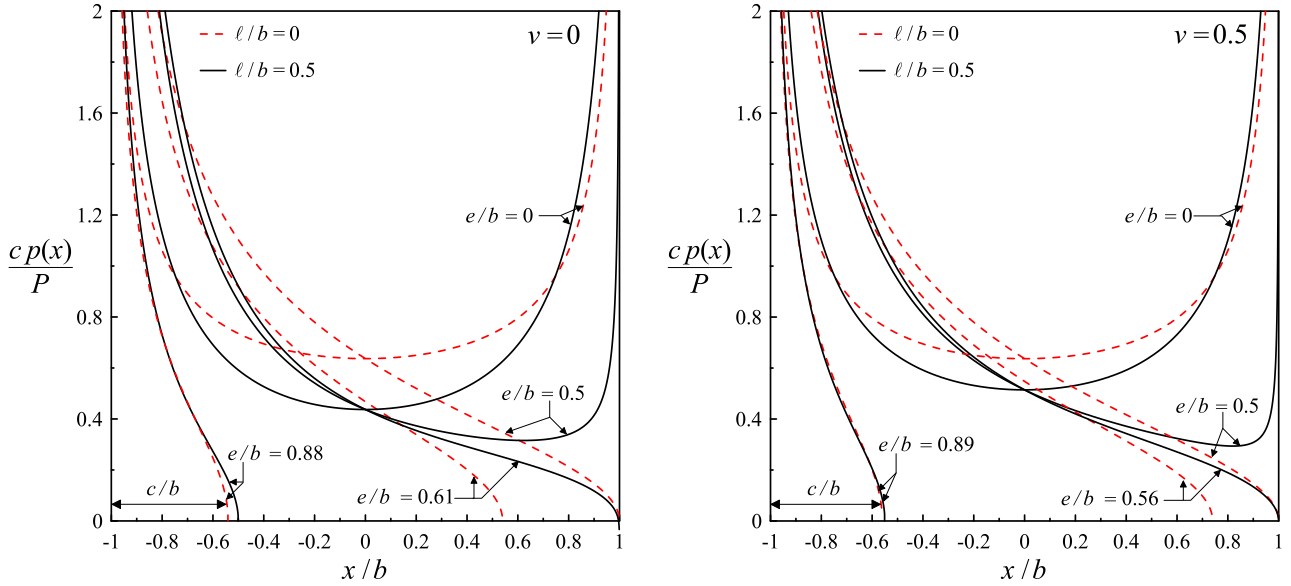

(a) **(b)**

Figure 2: The normalized pressure distribution $c\,p(x)/P$ as a function of the normalized distance x/b from the left corner of the indentor. Results are shown for two different Poisson's ratios (a) $\nu = 0$ and (b) $\nu = 0.5$.

5.2 Effect of the normalized characteristic length and the Poisson's ratio upon the limit eccentricity and the limit tilt angle

As it was shown by Sackfield et al. (2001) in the context of classical elasticity, if the force is positioned at a distance e from the punch center with $e \le b/2$, a *complete* contact of fixed extend will occur. In the case of couple-stress elasticity, the corresponding results become more complicated since the limit value of the load eccentricity between complete and receding contact varies also with the characteristic length ℓ of the material.

The dependence of the limit value of the normalized load eccentricity $e^{lim}/e^{lim}_{clas.}$ $(e^{lim}_{clas} = 0.5b)$ upon the normalized characteristic length ℓ/b is shown in Figure 3a. Interestingly, this dependence is *not* monotonous. In fact, it is observed that for very small values of the ratio ℓ/b (that is when the geometrical characteristics of the indentor are much larger than the material microstructure) the

response may be adequately described by the classical elasticity solution. As the ratio ℓ/b increases, the limit eccentricity exhibits a steep increase reaching a bounded maximum value at $\ell/b \approx 0.5$ independently of the Poisson's ratio. For $\nu = 0$ the maximum normalized limit eccentricity is $e^{lim}/e^{lim}_{clas.} = 1.22$, while for $\nu = 0.5$ the corresponding value is $e^{lim}/e^{lim}_{clas.} = 1.13$. As ℓ/b increases further, the limit eccentricity decreases monotonically and for $\ell/b \geq 10$ the classical elasticity results are essentially recovered.

The dependence of the limit value of the normalized tilt angle $\varphi^{lim}\mu b/P$ with respect to the normalized characteristic length ℓ/b is shown in Figure 3b. The classical limit value of the tilt angle is $\varphi^{lim}_{clas} = P(1-\nu)(\mu\pi b)^{-1}$ (Sackfield et al., 2001). It is observed that for $\ell/b = 0$ (dashed line), the classical elasticity results are recovered. For increasing ℓ/b the limit tilt angle decreases monotonically compared to the classical elasticity results and tends asymptotically to the values: 0.1 for $\nu = 0$, and 0.07 for $\nu = 0.5$, respectively.

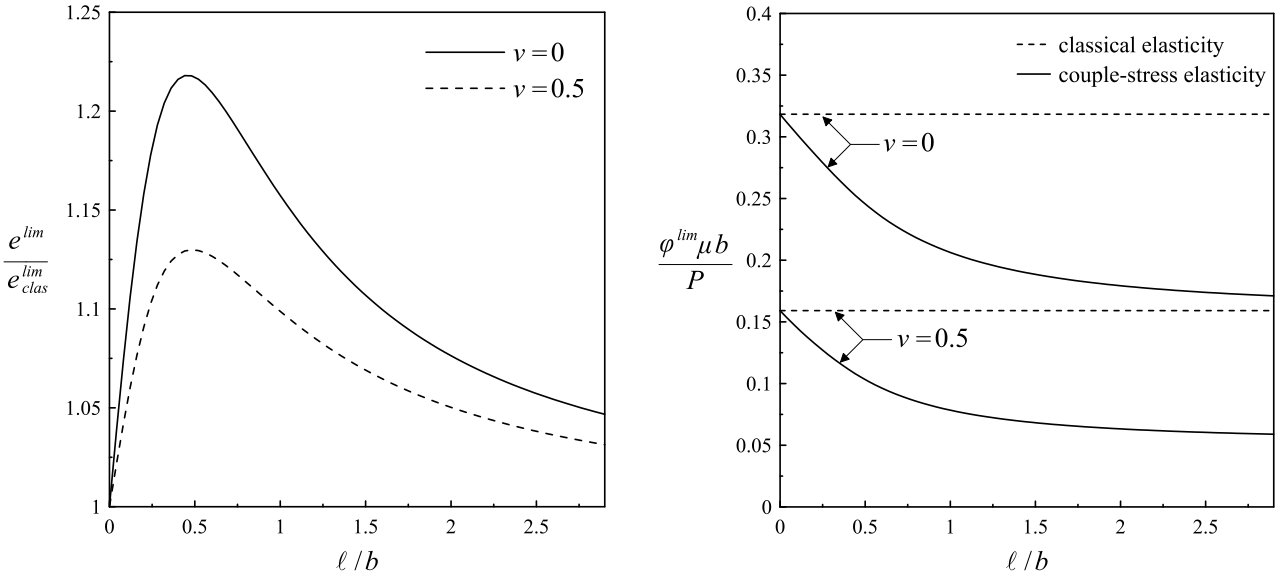

(a) **(b)**

Figure 3: The normalized limit (a) eccentricity $e^{lim}/e^{lim}_{clas.}$ and (b) tilt angle $\varphi^{lim}\mu b/P$, between normal and receding contact as a function of the normalized characteristic length ℓ/b.

In light of the above, it is concluded that *when the microstructure of the material is comparable to the width of the indentor an increased eccentricity (i.e. increased moment) with respect to classical elasticity is needed for the transition from complete to receding contact. On the*

other hand, the corresponding limit tilt angle decreases significantly compared to the classical elasticity result.

Moreover, Figure 4 illustrates the dependence of the normalized limit eccentricity $e^{lim}/e^{lim}_{clas.}$ and the normalized limit tilt angle $\varphi^{lim}\mu b/P$ upon the Poisson's ratio, respectively. In classical elasticity, the limit eccentricity does not depend upon the Poisson's ratio, while the limit tilt angle has a linear dependence upon ν. On the other hand, in couple-stress elasticity it is observed that for increasing Poisson's ratio the limit eccentricity decreases, for fixed values of ℓ/b (Fig. 4a). The maximum eccentricity is always attained at the value $\ell/b=0.5$ (envelope curve). Indeed, as ℓ/b increases, the ratio $e^{lim}/e^{lim}_{clas.}$ departs from unity (dashed line in Fig. 4a) approaching the envelope curve. As ℓ/b increases further, the limit eccentricity in couple-stress elasticity approaches again the classical limit. Finally, regarding the limit tilt angle, a monotonous decrease is observed with respect to the classical elasticity result for increasing ν and ℓ/b (Fig. 4b).

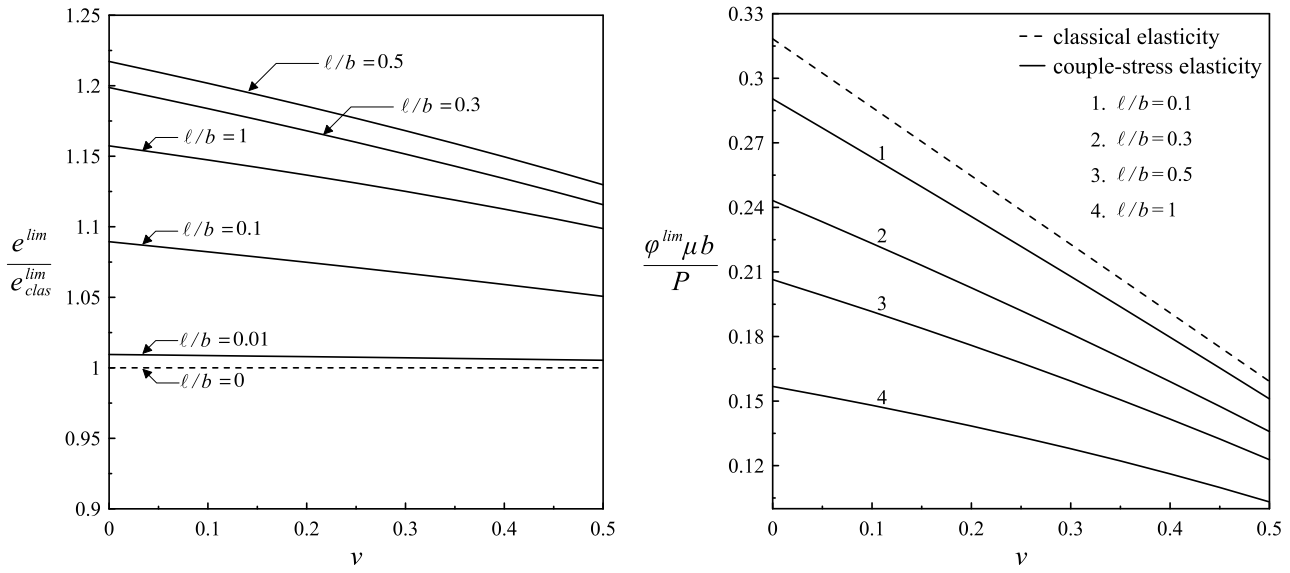

Figure 4: The normalized (a) limit eccentricity e^{lim}/e^{lim}_{clas} and (b) limit tilt angle $\varphi^{lim}\mu b/P$ as a function of the Poisson's ratio ν. Results are shown for selected values of ℓ/b.

The results of this section are summarized in Figures 5a and 5b where the dimensionless level sets of the limit eccentricity and the limit tilt angle are shown with respect to the Poisson's ratio ν and the microstructural ratio ℓ/b. From these plots one can directly extract the limit eccentricity and

the limit tilt angle for different levels of incompressibility and microstructural length scales. Conversely, given the width of the indentor $2b$, the Poisson's ratio ν, and the limit value of the eccentricity e^{lim} or the limit tilt angle φ^{lim}, one can extract information about the characteristic microstructural length ℓ.

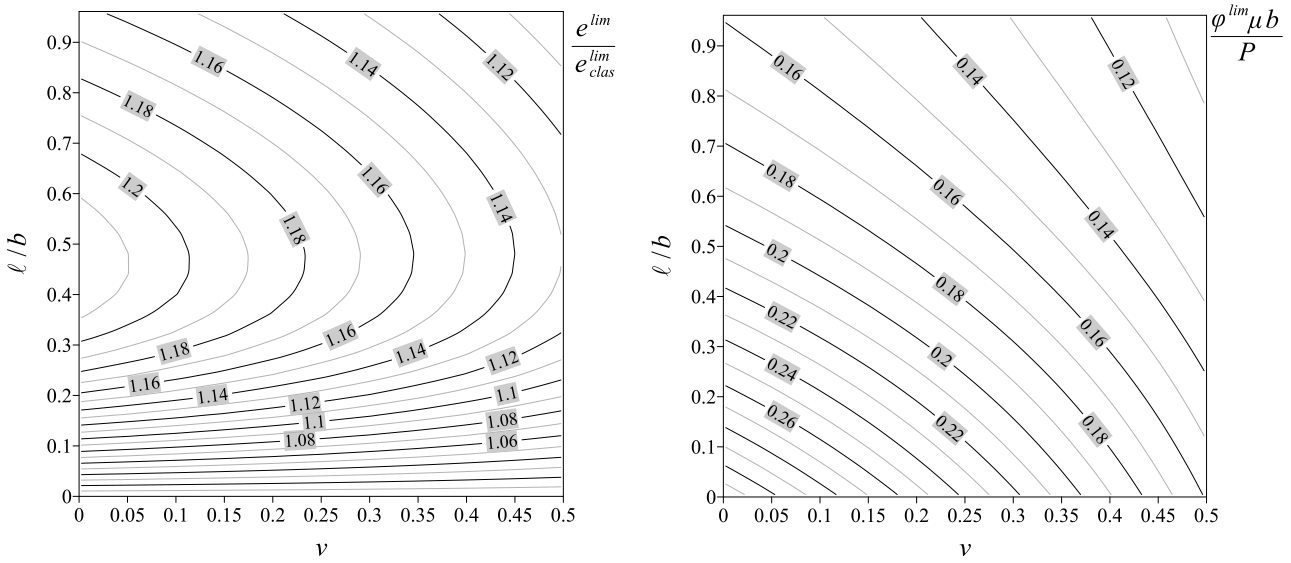

(a) **(b)**

Figure 5: Dimensionless level sets of (a) the limit eccentricity e^{lim}/e^{lim}_{clas}, and (b) the limit tilt angle $\varphi^{lim}\mu b/P$ as a function of the Poisson's ratio ν and the microstructural ratio ℓ/b.

5.3 Effect of the normalized eccentricity upon normalized tilt angle

Another important feature of the problem is the effect of the normalized eccentricity e/b (note that here the eccentricity is normalized with the contact half-width b) upon the normalized tilt angle $\varphi\mu b/P$. In Figure 6, this effect is analyzed for two different Poisson's ratios and a set of values of the ratio ℓ/b ranging from $\ell/b=0$ (classical elasticity) to $\ell/b=1$. It is shown that initially the contact is complete (light grey zone) and as the eccentricity of the applied load increases the contact becomes receding (dark grey zone) depending upon the ratio ℓ/b. The boundary between complete and receding contact is designated in the Figure 6 as '*limit from complete to receding contact*' (red line). It is readily observed that the tilt angles predicted by the classical elasticity are *larger* than those attained when couple-stress effects are considered for fixed load eccentricities. This finding implies that when couple-stress effects are taken into account a *stiffer* response is observed in terms of the tilt angle φ compared to the classical elasticity results. In the same figure, one should

note that the limit eccentricity for the transition from complete to receding contact, in the case of couple-stress elasticity, strongly depends upon the ratio ℓ/b and the Poisson's ratio ν. Nonetheless, regardless of the ratio ℓ/b as $e/b \to 1$, all the curves converge to each other (i.e. the dark shaded region gradually narrows) for all Poisson's ratios. This essentially suggests that the tilt angle φ for large load eccentricities is independent of the microstructural length.

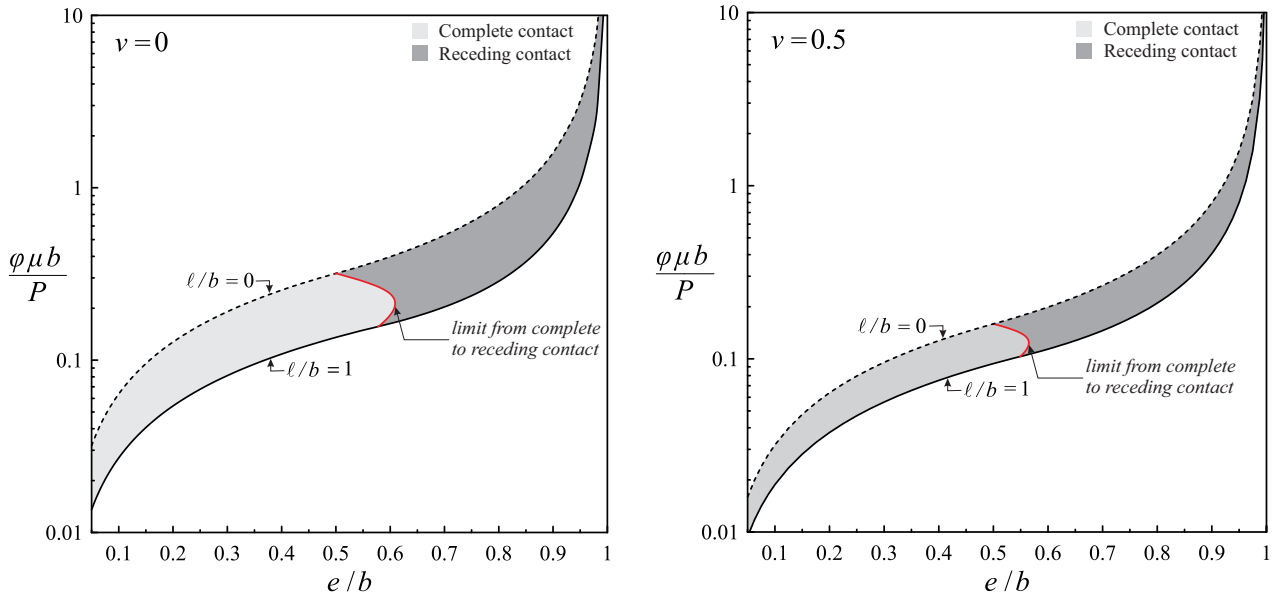

Figure 6: The normalized tilt angle $\varphi\mu b/P$ as a function of the normalized eccentricity e/b. Results are shown for two different Poisson's ratios (a) $\nu = 0$ and (b) $\nu = 0.5$.

5.4 Effect of the normalized eccentricity upon the normalized total contact area

The dependence of the total contact width upon the normalized eccentricity e/b and the characteristic length ℓ/b is investigated now for complete and receding contact conditions. The results are summarized in Figures 7a and 7b corresponding to Poisson's ratios $\nu = 0$ and $\nu = 0.5$, respectively. In the classical elasticity case ($\ell/b = 0$) the receding contact width c depends only upon the eccentricity of the applied load. In particular, when $e \le 0.5b$, the contact is complete independently of the Poisson's ratio and the magnitude of the applied load, and, thus, the normalized contact width $c/2b$ attains a constant value equal to unity. Further increase of the eccentricity suggests a linear reduction, $c = 4(b-e)$, of the contact region (Sackfield et al. 2001). On the other hand, for a couple-stress material the contact width c depends not only upon the eccentricity of the

applied load but also upon the microstructural ratio ℓ/b, and the Poisson's ratio ν. However, as in the classical elasticity case, the contact width is independent of the magnitude of the applied load P. For a material with $\nu=0$ and $\ell/b=0.5$ the contact is complete up to $e\le 0.61b$, beyond this limit the contact becomes receding and the contact width decreases in a nonlinear manner. The response is qualitatively similar for the case of Poisson's ratio $\nu=0.5$.

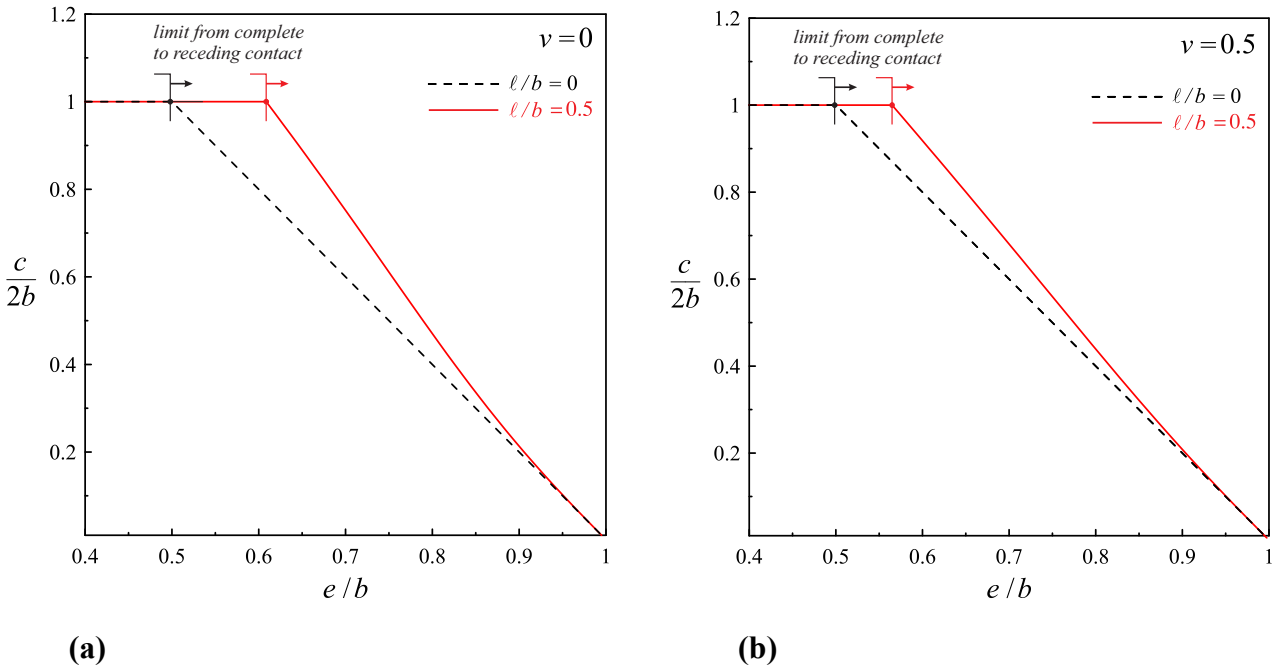

(a) **(b)**

Figure 7: The normalized contact width $c/2b$ as a function of the normalized eccentricity e/b. Results are shown for two different Poisson's ratios (a) $\nu=0$ and (b) $\nu=0.5$.

6. Conclusions

In the present study, a general solution has been derived for the two-dimensional plane strain tilted flat punch problem within the framework of the generalized continuum theory of couple-stress elasticity. This theory introduces a characteristic material length in order to describe the pertinent scale effects that emerge from the underlying microstructure and is capable of modeling complex microstructured materials. Our approach was based on singular integral equations which have resulted from a treatment of the mixed boundary value problems via integral transforms and generalized functions. The present results exhibit significant departure from the predictions of classical elasticity. In particular the following results were obtained:

- In couple-stress elasticity the limit value of the load eccentricity e^{lim} between complete and receding contact strongly depends upon the Poisson's ratio and the micromechanical length ℓ. This is in marked contrast with the classical elasticity case where the limit eccentricity is always $e^{lim}_{clas} = 0.5b$, independently of the Poisson's ratio. In both theories the limit value of the load eccentricity e^{lim} is independent of the magnitude of the applied load.
- The limit eccentricity e^{lim} is always increased when couple-stress effects are taken into account. The dependence between the limit eccentricity e^{lim} and the indent size ℓ/b is not monotonous, while the maximum limit eccentricity occurs for a material with $\ell/b \simeq 0.5$, regardless the value of the Poisson's ratio. This implies that when the microstructure of the material is comparable to the width of the indentor an increased eccentricity (i.e. a larger moment M compared to the classical elasticity result) is in need for the transition from complete to receding contact.
- The incorporation of the micromechanical internal length into the constitutive equations through couple-stress elasticity suggests a stiffer response in terms of the tilt angle φ when compared to the classical elasticity results. The tilt angle decreases both for increasing Poisson's ratio as well as increasing ℓ/b.
- In couple-stress elasticity, the receding contact width c depends upon the load eccentricity e (as in the classical theory), the microstructural ratio ℓ/b, and the Poisson's ratio ν. However, in both theories the contact width c is independent of the magnitude of the applied load. On the other hand, in contrast to the classical elasticity case, the reduction of the contact region in the receding contact regime is not a linear function of the load eccentricity.

Acknowledgement

Panos A. Gourgiotis gratefully acknowledges support from the ERC advanced grant 'Instabilities and nonlocal multiscale modelling of materials' under contract number FP7-PEOPLE-IDEAS-ERC-2013-AdG (2014-2019).

References

Bacca, M., Bigoni, D., Dal Corso, F., Veber, D. 2013. Mindlin second-gradient elastic properties from dilute two-phase Cauchy-elastic composites Part I: Closed form expression for the effective higher-order constitutive tensor. *International Journal of Solids and Structures* 50, 4010-4019.

Begley, M.R., Hutchinson, J.W., 1998. The mechanics of size-dependent indentation. *Journal of the Mechanics and Physics of Solids* 46, 2049-2068.

Bigoni, D., Drugan, W.J., 2007. Analytical Derivation of Cosserat Moduli via Homogenization of Heterogeneous Elastic Materials. *ASME Journal of Applied Mechanics* 74, 741-753.

Chen, X., Hutchinson, J.W., Evans, A.G., 2004. Simulation of the high temperature impression of thermal barrier coatings with columnar microstructure. *Acta Materialia* 52, 565-571.

Chen, J.Y., Huang, Y., Ortiz, M., 1998. Fracture analysis of cellular materials: A strain gradient model. *Journal of the Mechanics and Physics of Solids* 46, 789-828.

Erdogan F., Gupta G.D., Cook T.S., 1973. Numerical solution of singular integral equations. In: Sih G.C. (Ed). Mechanics of Fracture vol. 1: Methods of analysis and solutions of crack problems, 368–425

Erdogan, F., 1978. Mixed boundary-value problems in mechanics, in: Nemat-Nasser, S. (Ed.), Mechanics today. Pergamon Press, New York, pp. 1-86.

Fleck, N.A., Hutchinson, J.W., 2001. A reformulation of strain gradient plasticity *Journal of the Mechanics and Physics of Solids* 49, 2245-2271.

Fleck, N.A., Zisis, Th., 2010. The erosion of EB-PVD thermal barrier coatings: The competition between mechanisms. *Wear* 268, 1214-1224.

Gourgiotis, P.A., Piccolroaz, A. 2014. Steady-state propagation of a Mode II crack in couple stress elasticity. *International Journal of Fracture* 188, 119-145.

Han, C.-S., Nikolov, S., 2007. Indentation size effects in polymers and related rotation gradients. *Journal of Materials Research* 22, 1662-1672.

Hills, D.A., Nowell, D., Sackfield, A., 1993. Mechanics of Elastic Contact. Butterworth-Heinemann, Oxford.

Hills, D., Nowell, D., 1994. Mechanics of Fretting Fatigue. Kluwer Academic Publishers, Dordrecht.

Koiter, W., 1964. Couple stresses in the theory of elasticity. Parts I and II. *Proceedings of the Koninklijke Nederlandse Akademie van Wetenschappen* B67, 17-29.

Lakes, R.S., Gorman, D., Bonfield, W., 1985. Holographic screening method for microelastic solids. *Journal of Material Science* 20, 2882–2888.

Larsson, P. L., Giannakopoulos, A. E., Söderlund, E., Rowcliffe, D. J., Vestergaard, R., 1996. Analysis of Berkovich indentation *International Journal of Solids and Structures* 33, 221-248.

Maranganti, R., Sharma, P., 2007. A novel atomistic approach to determine strain-gradient elasticity constants: Tabulation and comparison for various metals, semiconductors, silica, polymers and the

(Ir) relevance for nanotechnologies. *Journal of the Mechanics and Physics of Solids* 55, 1823-1852.

Mindlin, R.D., Tiersten, H.F., 1962. Effects of couple-stresses in linear elasticity. *Archive for Rational Mechanics and Analysis* 11, 415-448.

Mindlin, R.D., 1963. Influence of couple-stresses on stress concentrations. *Experimental Mechanics* 3, 1-7.

Muki, R., Sternberg, E., 1965. The influence of couple-stresses on singular stress concentrations in elastic solids. *Zeitschrift für angewandte Mathematik und Physik ZAMP* 16, 611-648.

Nix, W.D., Gao, H., 1998. Indentation size effects in crystalline materials: A law for strain gradient plasticity. *Journal of the Mechanics and Physics of Solids* 46, 411-425.

Poole, W.J., Ashby, M.F., Fleck, N.A., 1996. Micro-hardness of annealed and work-hardened copper polycrystals. *Scripta Materialia* 34, 559-564.

Sackfield, A., Truman, C.E., Hills, D.A., 2001. The tilted punch under normal and shear load (with application to fretting tests). *International Journal of Mechanical Sciences* 43, 1881-1892.

Shodja, H.M., Zaheri, A., Tehranchi, A., 2013. Ab initio calculations of characteristic lengths of crystalline materials in first strain gradient elasticity. *Mechanics of Materials* 61, 73-78.

Shu, J.Y., Fleck, N.A., 1998. The prediction of a size effect in microindentation. *International Journal of Solids and Structures* 35, 1363-1383.

Stupkiewicz, S., 2007. Micromechanics of contact and interphase layers. Lecture Notes in Applied and Computational Mechanics, vol. 30. Springer, Berlin.

Szegö, 1939. Orthogonal Polynomials, Colloquium Publications, 23. American Mathematical Society.

Tekoglu, C. Onck, P.R., 2008. Size effect sin two dimensional Voronoi foams. A comparison between generalized continua and descrite models. *Journal of the Mechanics and Physics of Solids* 56, 3541-3564.

Toupin, R.A., 1964. Theories of elasticity with couple-stress. *Archive for Rational Mechanics and Analysis* 17, 85-112.

Wei, Y., Hutchinson, J.W., 2003. Hardness trends in micron scale indentation. *Journal of the Mechanics and Physics of Solids* 51, 2037-2056.

Zisis, Th., Fleck, N.A., 2010. The elastic–plastic indentation response of a columnar thermal barrier coating. *Wear* 268, 443-454.

Zisis, Th., Gourgiotis, P.A., Baxevanakis, K.P., Georgiadis, H.G., 2014. Some basic contact problems in couple-stress elasticity. *International Journal of Solids and Structures* 51, 2084–2095.